Modular Multilevel Converter Based Induction Machine Drive

Yin Li, *Student Member, IEEE*, Lingling Fan, *Senior Member, IEEE*

***Abstract*—This paper proposes that a medium voltage level power Modular Multilevel Converter (MMC) based induction machine drive. MMC replaces a two-level voltage source converter (VSC) to drive an induction motor because of its high voltage power range. A designed 5-level three-phase dc-to-ac MMC is analyzed on the circular topology. The indirect field orientated vector control (FOC) is used to control the motor. This paper also compares the vector control loops with a constant and a dynamic rotor flux as feedforward. The motor drive system is simulated in MATLAB/SimPowerSystems. The simulation results validate the control design of the motor drive with two different vector control loops.**

***Index Terms*—Modular multilevel converter, field orientation vector control, constant and dynamic rotor flux.**

I. Introduction

With the rapid development of the high-voltage power applications, a newer kind of VSC, modular multilevel converter (MMC) has been applied in HVDC systems [1], [2]. Till now, MMC is used more and more widely in industrial area. In the renewable energy market, MMC can replace a two-level or three-level VSC to drive a wind machine [3]. Study on motor drive with MMC in this paper can be applied to wind farms. Compared with the traditional two-level VSC, the MMC contains more than one sub-module (SM) in cascaded connection on each arm [4]. The structure of a three-phase dc-to-ac MMC with a detailed sub-module is shown in Fig.1. The sub-module is a simple buck converter with two IGBT and a dc capacitor, C_{sm}. MMC has two main advantages due to its special structure. First, the cascaded connection of sub-modules makes the MMC intended for any voltage power level requirement, especially for the medium and high voltage power applications [4]–[6]. Second, the high-level number of the submodules can reduce the effect of the harmonic distortion and the switching frequency [7]–[9]. For simulation based studies, MMC has a drawback on simulation time. The huge number of sub-modules corresponds to the huge effort of computation. Therefore, for simulation studies, the range of the number of sub-modules in many experiments is from 2 to 8 [1], [2], [10]–[12]. In this paper, a 5-level MMC is chosen.

Indirect field oriented vector control (FOC) [13] is very popular in motor drives. It can overcome the inherent coupling effect in scalar control and realize torque/flux control speedily. The vector control is based on the rotor flux reference frame where d-axis is aligned with the rotor flux. The rotor flux may be considered as a constant due to flux control. The response speed is relative slow in the outer control loop of the FOC, so this assumption can be used when designing the inner loop. Nevertheless, the fast response speed of the inner loop will cause this assumption not to be rigorous. In this paper, two kinds of the inner loops are compared based on with or without a constant rotor flux assumption.

Y. Li and L. Fan are with Dept. of Electrical Engineering, University of South Florida, Tampa FL 33620. Emails: yin@mail.usf.edu, linglingfan@usf.edu.

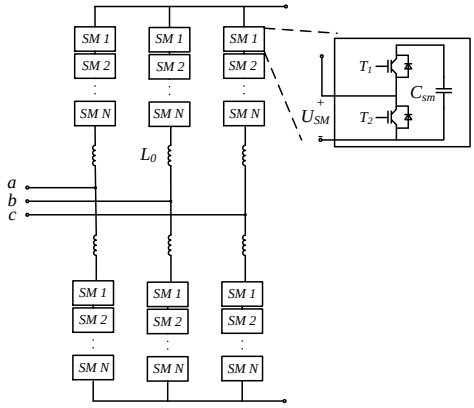

Fig. 1. The basic structure of three-phase MMC with the sub-module.

This paper addresses two main issues. One is to test MMC's control performance on motor drive. Another is if a vector control considering a dynamic rotor flux is better than one with a constant rotor flux. The following sections will analyze the basic structure and the circular interactions of the MMC. They also explain how two kinds of the vector control loop is designed and compared. Simulation results in Matlab/SimPowerSystems are given.

II. MMC topology and control structure

Fig.1 shows the topology of a three-phase dc-to-ac modular multilevel converter. The right side is the input of MMC which should be connected to a dc power supply. The output of MMC is on the left side and can be applied to a three-phase grid application. Because it is a three-phase converter, there are six arms and each of them contains a group of the cascade connected sub-modules. The number of sub-modules, N, is depended on the specific voltage level requirement. On each arm , there is also an inductor marked L_0 which can filter some high-order harmonics from the circulating current. Its value cannot be too high because of the large voltage drop and high cost of high-voltage inductor, although the high inductance can reduce the amplitude of one undesired component of the arm current, the circulating current [5].

In this section, the analysis uses Phase A as the example. Fig.2 shows the two equivalent circuits of Phase A to analyze the circular interactions. Phase A has two arms, so i_{ap} and i_{an} are denoted as the upper and lower arm currents which contains two parts. One is inner current which just flows inside the phase unit, $i_{diff,a}$, and another one is the MMC output current, i_{a_grid}, shown in Fig.2 b). Because i_{ap} and i_{an} are symmetric, i_{a_grid} is divided equally into each of them. Therefore, due to KCL, i_{ap} and i_{an} can be expressed as

$$\begin{cases} i_{ap}(t) = \frac{i_{a\_grid}}{2} + i_{diff,a} \\ i_{an}(t) = -\frac{i_{a\_grid}}{2} + i_{diff,a} \end{cases} \tag{1}$$

Moreover, i_{a_grid} is a sinusoidal wave with the fundamental frequency to supply the grid application and $i_{diff,a}$ includes a dc component, I_{ad}, and the circulating current with high-order harmonics, i_{cir}.

The voltage dropping on each arm inductor, L_0, is caused by $i_{diff,a}$, and it is named as the inner unbalanced voltage, $u_{diff,a}$. Based on KVL and Fig.2 a), the arm voltages can be expressed as

$$\begin{cases} u_{ap} = \frac{U_{dc}}{2} - L_0 \frac{di_{diff,a}}{dt} - v_{a\_grid} \\ u_{an} = \frac{U_{dc}}{2} - L_0 \frac{di_{diff,a}}{dt} + v_{a\_grid} \end{cases} \tag{2}$$

where U_{dc} is the dc voltage source and v_{a_grid} is the output voltage of the MMC. The sum of the upper and lower arm voltages should be equal to the dc voltage source. The half of the difference between them is the output voltage, v_{a_grid}, and it is also named as the inner emf, e_a. It is used as the control voltage in vector control. An additional control block to suppress the circulating current is also included to adjust e_{diff}. Interested readers can refer [2] for a comparison on control structures of a two-level VSC and MMC. For motor control, e_{abc} will be the final controller output from the FOC.

$$\begin{cases} u_{an} + u_{aa} = U_{dc} + 2u_{diff,a} \\ \frac{u_{an} - u_{ap}}{2} = v_{a\_grid} = e_a \end{cases} \tag{3}$$

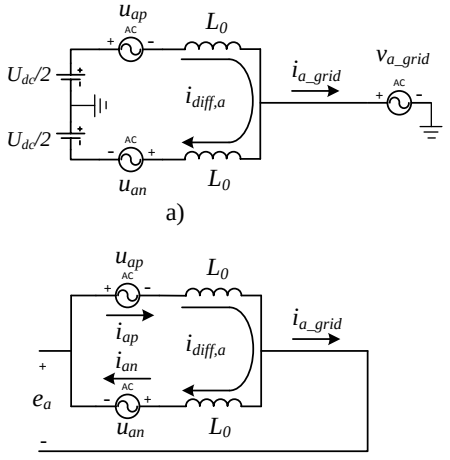

Fig. 2. a) the equivalent circuit for u_{an}+u_{ap}; b) the equivalent circuit for u_{an}-u_{ap}

III. The Rotor Field Orientated Vector Control

The whole motor drive system is designed like Fig.3. The bottom part is the control loop which has the outer control loop and the inner control loop. The outer loop is controlled by the rotor flux and frequency. The inner loop is controlled by the stator current. How the control loop is designed will be analyzed in this section. The superscript of the current or flux, s or e, means the stationary frame or synchronous frame. The subscript, s or r, means stator side and rotor side. The subscript, q or d, means the components on q-axis or d-axis. The values measured from the induction motor in SimPowerSystems are: φ^s_{qr}, φ^s_{dr}, i^s_{qs}, i^s_{ds} and ω_r shown in Fig.3.

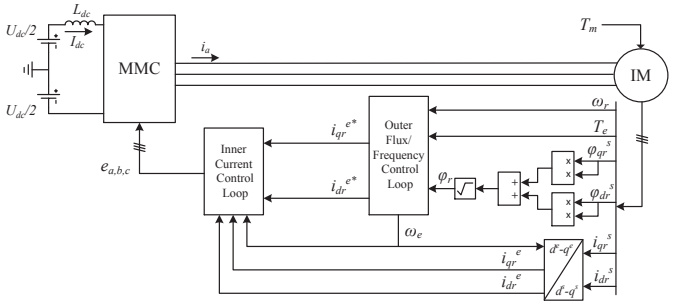

Fig. 3. Motor The whole motor drive system with MMC

A. Outer Flux and Frequency Control

First, the relation between the rotor flux and the stator current should be derived. The flux linkage expressions in terms of the currents can be written as follows:

$$\varphi^e_{qs} = L_{ls} i^e_{qs} + L_m (i^e_{qs} + i^e_{qr}) = L_s i^e_{qs} + L_m i^e_{qr} \tag{4a}$$
$$\varphi^e_{ds} = L_{ls} i^e_{ds} + L_m (i^e_{ds} + i^e_{dr}) = L_s i^e_{ds} + L_m i^e_{dr} \tag{4b}$$
$$\varphi^e_{qr} = L_{lr} i^e_{qr} + L_m (i^e_{qs} + i^e_{qr}) = L_r i^e_{qr} + L_m i^e_{qs} \tag{4c}$$
$$\varphi^e_{dr} = L_{lr} i^e_{qr} + L_m (i^e_{ds} + i^e_{dr}) = L_r i^e_{dr} + L_m i^e_{ds} \tag{4d}$$

where L_{ls} and L_{lr} are the stator and rotor inductance, L_m is the mutual inductance, L_s=L_{ls}+L_m, and L_r=L_{lr}+L_m.

The rotor circuit equation in dq reference frame is:

$$\overline{e^e_r} = 0 = R_r \overline{I^e_r} + \frac{d}{dt}\overline{\varphi^e_r} + j\omega_{sl}\overline{\varphi^e_r} \tag{5}$$

where ω_{sl} is the slip frequency.

When the equation is converted into d and q components shown in Fig.4, (5) can be written:

$$\begin{aligned} 0 = e^e_{qr} &= R_r i^e_{qr} + \frac{d}{dt}\varphi^e_{qr} + \omega_{sl}\varphi^e_{dr} \\ 0 = e^e_{dr} &= R_r i^e_{dr} + \frac{d}{dt}\varphi^e_{dr} - \omega_{sl}\varphi^e_{qr} \end{aligned} \tag{6}$$

To replace the rotor current in (6), (4c) and (4d) can be also expressed:

$$\begin{aligned} i^e_{qr} &= \frac{1}{L_r}\varphi^e_{qr} - \frac{L_m}{L_r} i^e_{qs} \\ i^e_{dr} &= \frac{1}{L_r}\varphi^e_{dr} - \frac{L_m}{L_r} i^e_{ds} \end{aligned} \tag{7}$$

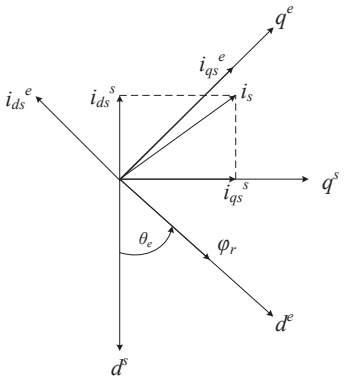

Fig. 4. Stationary frame d^s-q^s to synchronous rotating frame d^e-q^e transformation

Substituting (7) into (6):

$$\begin{aligned} 0 &= \frac{d\varphi_{qr}^e}{dt} + \frac{R_r}{L_r}\varphi_{qr}^e - \frac{L_m L_r}{R_r} i_{qs}^e + \omega_{sl}\varphi_{dr}^e \\ 0 &= \frac{d\varphi_{dr}^e}{dt} + \frac{R_r}{L_r}\varphi_{dr}^e - \frac{L_m L_r}{R_r} i_{ds}^e + \omega_{sl}\varphi_{qr}^e \end{aligned} \tag{8}$$

It is assumed that the rotor flux, $\hat{\varphi}_r$, is constant due to it slowly response, the differential of the rotor flux is zero. Then, the indirect rotor field orientation control strategy is considered in this study (φ_{qr}^e=0, φ_{dr}^e=$\hat{\varphi}_r$), so (8) can be rewritten as:

$$\omega_{sl} = \frac{R_r L_m}{\hat{\varphi}_r L_r} i_{qs}^e \tag{9}$$

$$\hat{\varphi}_r = \varphi_{dr}^e = L_m i_{ds}^e \tag{10}$$

The rotor flux is from two measured components.

$$\hat{\varphi}_r = \sqrt{(\varphi_{qr}^s)^2 + (\varphi_{dr}^s)^2} \tag{11}$$

θ_e shown in Fig.4 is synchronous frequency angle combined with ω_{sl} and ω_r.

$$\theta_e = \int \omega_e = \int (\omega_r + \omega_{sl}) dt \tag{12}$$

1) PI Controller Design For the Frequency Control: The relation between T_e and ω_r can be expressed:

$$T_e - T_m = J\frac{d\omega_r}{dt} + B\omega_r \tag{13}$$

where J is the inertia and B is the friction factor. T_m is the desired load torque which is zero when designing the PI controller, so the plant model for $\frac{\omega_r}{T_e}$ is $\frac{1}{Js+B}$ (s is the differential operator). To design the PI controller, the open loop transform function is:

$$\begin{aligned} \left(K_p + \frac{K_i}{s}\right) G(s) &= \frac{K_p s + K_i}{s} \frac{1}{Js+B} \\ &= \frac{K_p}{Js} \frac{s + \frac{K_i}{K_p}}{s + \frac{B}{J}} \end{aligned} \tag{14}$$

where $G(s)$ is used to present the plant model. For stabilizing the feedback control loop, the pole should be canceled using the zero of PI compensator.

$$\begin{cases} \frac{K_i}{K_p} &= \frac{B}{J} \\ \frac{K_p}{J} &= \frac{1}{\tau_{te}} \end{cases} \Rightarrow \begin{cases} K_p &= \frac{J}{\tau_{te}} \\ K_i &= \frac{B}{\tau_{te}} \end{cases} \tag{15}$$

where τ_{te} is the time constant for T_e PI controller. Therefore, a determined τ_{te} can determine K_p first; then, K_i will be calculated based on K_p.

2) PI Controller Design For the Torque Control: Because of φ_{qr}^e=0, φ_{dr}^e=$\hat{\varphi}_r$, and $\hat{\varphi}_r$ is considered as a constant, the electric torque, T_e, is proportional to i_{qs}^e (in my case, rotor flux is around 0.25Wb).

$$T_e = \frac{3}{4}P(i_{qs}^e \varphi_{dr}^e - i_{ds}^e \varphi_{qr}^e) = \frac{3P\hat{\varphi}_r}{4} i_{qs}^e \tag{16}$$

where P is the number of poles. The plant model is $\frac{3P\hat{\varphi}_r}{4}$ which is a pure gain. Based on it, the closed-loop transfer function is:

$$\begin{aligned} T(s) &= \frac{\frac{K_p s + K_i}{s} G(s)}{1 + \frac{K_p s + K_i}{s} G(s)} = \frac{\frac{G(s)K_p}{K_i} s + 1}{\tau_{out} s + 1} \\ \tau_{out} &= \frac{G(s)K_p + 1}{G(s)K_i} = \frac{0.75K_p + 1}{0.75K_i} \\ K_p &= \frac{0.75\tau_{out}K_i - 1}{0.75} \end{aligned} \tag{17}$$

where τ_{out} is the outer loop time constant (for both $\hat{\varphi}_r$ and T_e). When the time constant and K_i are determined, K_p can be calculated.

3) PI Controller Design For the Flux Control: Due to (10), the plant model is a pure gain, L_m; then the transfer function is:

$$\begin{aligned} T(s) &= \frac{\frac{K_p s + K_i}{s} L_m}{1 + \frac{K_p s + K_i}{s} L_m} = \frac{\frac{K_p}{K_i} s + 1}{\tau_{out} s + 1} \\ \tau_{out} &= \frac{L_m K_p + 1}{L_m K_i} \\ K_p &= \frac{L_m \tau_{out} K_i - 1}{L_m} \end{aligned} \tag{18}$$

K_p is determined after determining the time constant and K_i.

Finally, the closed loops related to frequency and flux control are shown in Fig.5. The controller parameters can be found in Tables 1-3.

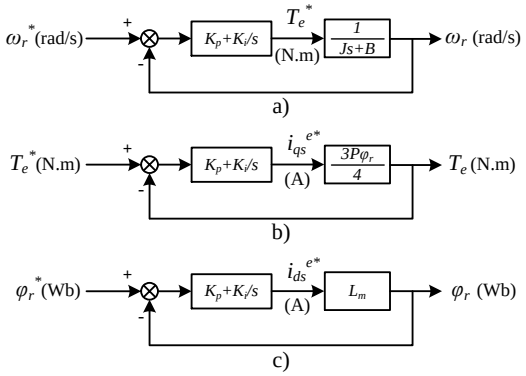

Fig. 5. The closed loops related to a) ω_r, b) T_e, and c) $\hat{\varphi}_r$.

B. Inner Current Control Loop

In the inner current loops, the stator current in the synchronous frame is used to control the reference stator voltage. Hence, the relation between the stator current and voltage should be derived before designing the PI controllers. The input voltage of the induction motor in a stationary frame can be represented by a space vector.

$$\vec{e_s^s} = R_s \vec{I_s^s} + \frac{d}{dt}\vec{\varphi_s^s} \tag{19}$$

Transforming (19) to a synchronous frame (ω_e):

$$\bar{e_s^e} = R_s \bar{I_s^e} + \frac{d}{dt}\bar{\varphi_s^e} + j\omega_e \bar{\varphi_s^e} \tag{20}$$

Separating (20) into d-q components:

$$\begin{cases} e_{qs}^e = R_s i_{qs}^e + \frac{d}{dt}\varphi_{qs}^e + \omega_e \varphi_{ds}^e \\ e_{ds}^e = R_s i_{ds}^e + \frac{d}{dt}\varphi_{ds}^e - \omega_e \varphi_{qs}^e \end{cases} \tag{21}$$

To express φ_{ds}^e and φ_{qs}^e, (4c) and (4d) are substituted into (4a) and (4b).

$$\begin{cases} \varphi_{qs}^e = L_s i_{qs}^e + L_m \frac{\varphi_{qr}^e - L_m i_{qs}^e}{L_r} = \sigma L_s i_{qs}^e + \frac{L_m}{L_r}\varphi_{qr}^e \\ \varphi_{ds}^e = L_s i_{ds}^e + L_m \frac{\varphi_{dr}^e - L_m i_{ds}^e}{L_r} = \sigma L_s i_{ds}^e + \frac{L_m}{L_r}\varphi_{dr}^e \end{cases} \tag{22}$$

where σ=1 $- \frac{L_m^2}{L_s L_r}$.

Like in the outer loop, $\hat{\varphi_r}$ is also assumed as a constant in the inner loop, so (10) can be applied here. Moreover, due to the rotor flux, φ_{qr}^e=0 and (10) are substituted into (22),

$$\begin{cases} \varphi_{qs}^e &= \sigma L_s i_{qs}^e \\ \varphi_{ds}^e &= \sigma L_s i_{ds}^e + \frac{L_m}{L_r} L_m i_{ds}^e = L_s i_{ds}^e \end{cases} \tag{23}$$

To use the current to replace the flux linkage in (21), (23) is substituted into (21):

$$\begin{cases} e_{qs}^e = R_s i_{qs}^e + \frac{d}{dt}\sigma L_s i_{qs}^e + \omega_e L_s i_{ds}^e \\ e_{ds}^e = R_s i_{ds}^e + \frac{d}{dt} L_s i_{ds}^e - \omega_e \sigma L_s i_{qs}^e \end{cases} \tag{24}$$

To define virtual voltages, u_{qs}^e and u_{ds}^e, (24) can be rewritten:

$$\begin{cases} u_{qs}^e = e_{qs}^e - \omega_e L_s i_{ds}^e = (R_s + \sigma L_s s) i_{qs}^e \\ u_{ds}^e = e_{ds}^e + \omega_e \sigma L_s i_{qs}^e = (R_s + L_s s) i_{ds}^e \end{cases} \tag{25}$$

Based on (25), the plant models for the q-axis and d-axis current control are $\frac{1}{\sigma L_s s + R_s}$ and $\frac{1}{L_s s + R_s}$. They are used to design the PI controllers for the current control.

1) PI Controller Design For q-axis Current Control : The open loop transfer function:

$$\left(K_p + \frac{K_i}{s}\right) G(s) = \frac{K_p}{\sigma L_s s} \frac{s + \frac{K_i}{K_p}}{s + \frac{R_s}{\sigma L_s}} \tag{26}$$

Using the same way used for T_e to determine K_p and K_i:

$$\begin{cases} K_p &= \frac{\sigma L_s}{\tau_{in}} \\ K_i &= \frac{R_s}{\tau_{in}} \end{cases} \tag{27}$$

where τ_{in} is the time constant for the inner loop.

2) PI Controller Design For d-axis Current Control: The plant model for the d-axis is different.

$$\left(K_p + \frac{K_i}{s}\right) G(s) = \frac{K_p}{L_s s} \frac{s + \frac{K_i}{K_p}}{s + \frac{R_s}{L_s}} \tag{28}$$

$$\begin{cases} K_p &= \frac{L_s}{\tau_{in}} \\ K_i &= \frac{R_s}{\tau_{in}} \end{cases} \tag{29}$$

The closed loops related to the current control are shown in Fig.6.

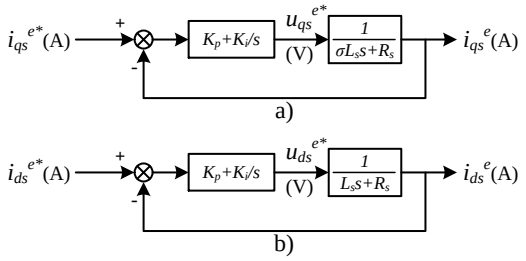

Fig. 6. The closed loops related to a) q-axis current control and b) d-axis current control

A coupling operation has to be used in the control loop to produce the final desired reference voltages, e_{qs}^e and e_{ds}^e (25). Therefore, the whole control system is shown in Fig.7.

Actually, the much faster response speed of the inner loop causes that the effect of $\frac{d\varphi_{dr}^e}{dt}$ cannot be neglected. Therefore, considering a dynamic $\hat{\varphi_r}$ is a better and more accurate way to design the inner control loop. As a result, (10) cannot be substituted into (22). (23) is replaced by the following expression.

$$\begin{cases} \varphi_{qs}^e = \sigma L_s i_{qs}^e \\ \varphi_{ds}^e = \sigma L_s i_{ds}^e + \frac{L_m}{L_r}\hat{\varphi_r} \end{cases} \tag{30}$$

Substituting (30) into (21),

$$\begin{cases} e_{qs}^e = R_s i_{qs}^e + \frac{d}{dt}\sigma L_s i_{qs}^e + \omega_e L_s i_{ds}^e + \omega_e \frac{L_m}{L_r}\hat{\varphi_r} \\ e_{ds}^e = R_s i_{ds}^e + \frac{d}{dt}\sigma L_s i_{ds}^e - \omega_e \sigma L_s i_{qs}^e \end{cases} \tag{31}$$

The virtual voltages should be redefined based on (31).

$$\begin{cases} u_{qs}^e = e_{qs}^e - \omega_e L_s i_{ds}^e - \omega_e \frac{L_m}{L_r}\hat{\varphi_r} = (R_s + \sigma L_s s) i_{qs}^e \\ u_{ds}^e = e_{ds}^e + \omega_e \sigma L_s i_{qs}^e = (R_s + \sigma L_s s) i_{ds}^e \end{cases} \tag{32}$$

(32) shows that the plant models for the new inner current control are the same as it for q-axis current control in the previous inner control, $\frac{1}{\sigma L_s s + R_s}$, so the determined K_p and K_i from (29) can be also applied for both dq current control in the new inner loop. However, e_{qs}^e is coupled with one more component, $\omega_e \frac{L_m}{L_r}\hat{\varphi_r}$ (31), so the new structure of the inner loop is improved shown by the red dash line parts in Fig. 7.

IV. Simulation Results from MATLAB/SimPowerSystems

To verify that the MMC can replace the traditional VSC to drive an induction motor with the vector control, a detailed model is developed in the SimPowerSystems of MATLAB. Fig.3 shows the structure of the simulated system. Between

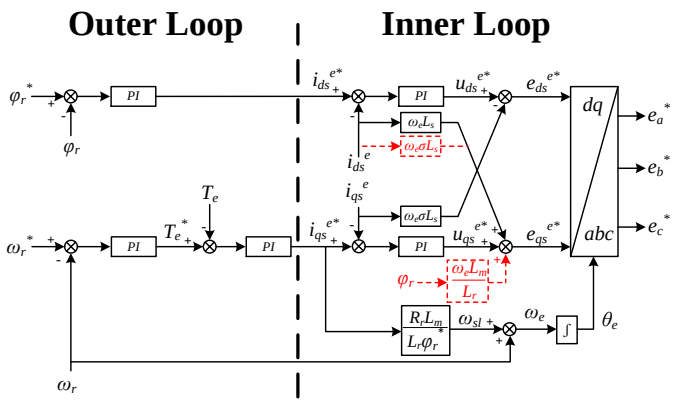

Fig. 7. The structure of the vector control system (The red dash line parts are the improvements for the dynamic $\hat{\varphi}_r$).

TABLE I

Parameter	Value
Rated DC-link voltage of MMC	250V
Arm inductance L_0	0.002H
DC side inductance L_{dc}	0.005H
Number of submodules of each arm (N)	4
Capacitance of each sub-module (C_{sm})	2.5mF
Switching frequency	1050Hz

DC voltage source and MMC, there is a dc inductor which filters some harmonics of the dc current. The main values of the MMC are listed in Table 1 and the values of the induction motor are listed in Table 2. The values for the designed PI controllers are determined by the equations in Section III listed in Table 3.

TABLE II

Parameter	Value
Nominal power, voltage(rms,line-line)	2238VA, 220V
Nominal frequency	60Hz
Stator resistance (R_s), inductance (L_s)	0.435Ω, 0.002H
Rotor resistance (R_r), inductance (L_r)	0.816Ω, 0.002H
Mutual inductance (L_m)	69.31× 10^{-3} H
Inertia (J)	0.089Kg.m^2
Friction factor (B), poles (P)	0.005N.m.s, 4

TABLE III

	Constant $\hat{\varphi}_r$			Dynamic $\hat{\varphi}_r$		
Control	τ	K_p	K_i	τ	K_p	K_i
ω_r	40ms	2.225	0.125	40ms	2.225	0.125
T_e	10ms	0.367	170	10ms	0.367	170
$\hat{\varphi}_r$	10ms	5.572	2000	10ms	5.572	2000
i^e_{qs}	1ms	3.944	435	1ms	3.944	435
i^e_{ds}	1ms	71.31	435	1ms	3.944	435

During the simulation, there are three variables changed separately. The total simulation time is 10 second. Before 1s, the induction motor sped up. At 2s, T_m had a step response from 0 to 10N.m. T_e is always following the variation of T_m, so in another word, T_e was increased to 10N.m from 0 at 2s. The corresponding response of each PI controller's input is shown in Fig.8. The black dash line presents the response speed of the system. It is located at 0.04s after the step response (τ_{te}=0.04s). The left side is the plot related to a constant $\hat{\varphi}_r$ and the right side is related to a dynamic one. Because i^e_{qs} is related to T_e, the step response of T_e just causes i^e_{qs} increase and other parameters kept the constant with a transient. After comparing both side, the right rotor flux plot had a smaller response than the left one.

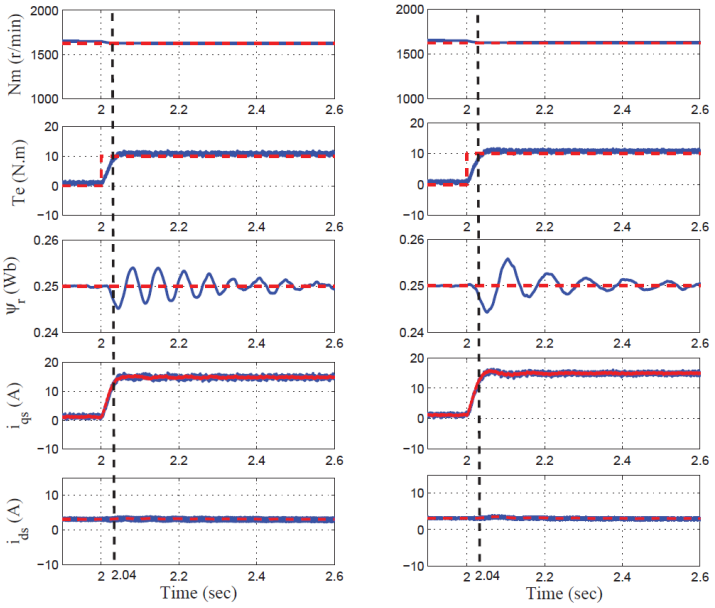

Fig. 8. At 2s, T_e is changed from 0 to 10N.m. Constant $\hat{\varphi}_r$ (left); dynamic $\hat{\varphi}_r$ (right). Dotted red line (reference); solid blue line (measurement)

At 5s, the rotor speed, N_r, was reduced to 1432 from 1623r/min. In Fig. 9. It is observed that other PI controllers' inputs kept the constant when Nr was changed. Although it is related to N_r, T_e always follows T_m which is constant after 2s. Fig.9 proves that T_e is independent to N_r and $\hat{\varphi}_r$. Moreover, the right plots had a obviously faster and smaller response than the left.

At 8s, a step response happened on $\hat{\varphi}_r$ which was increased to 0.35 from 0.25Wb. In Fig.10, i^e_{ds} was increased a little because its reference is the output of $\hat{\varphi}_r$. The decrease of i^e_{qs} can be explained by (16). When T_e and P are constant, i^e_{qs} is inversely proportional to $\hat{\varphi}_r$. In Fig.10, the right plots also had the faster and smaller response.

In a conclusion, the figures shows when the value of one variable among T_e, N_r, and $\hat{\varphi}_r$, was changed, the other two kept the constant with a short transient. It is [proved that the vector control loops of these two systems with a MMC worked well because the three variables can be controlled independently of each other. However, it is observed that the right side plots had a faster and smaller response than the left ones, hence, the vector control loop considering a dynamic $\hat{\varphi}_r$ works better than one assuming a constant flux.

V. Conclusion

As a kind of converter more applied for the medium and high voltage power applications, a 5-level MMC is used to

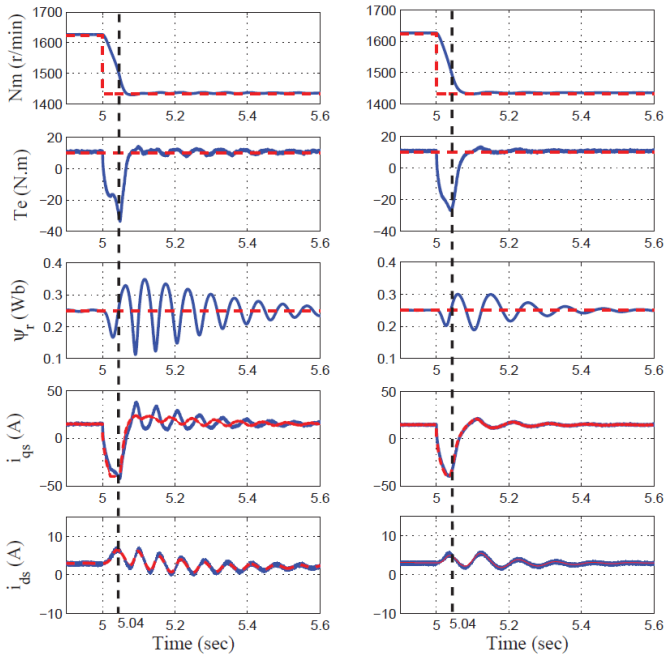

Fig. 9. At 5s, N_r is changed from 1623 to 1432r/min. Constant $\hat{\varphi_r}$ (left); dynamic $\hat{\varphi_r}$ (right). Dotted red line (reference); solid blue line (measurement)

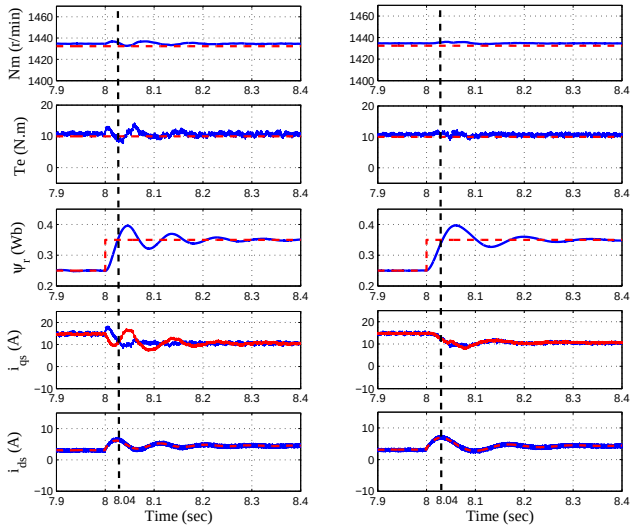

Fig. 10. At 8s, $\hat{\varphi_r}$ is changed from 0.25 to 0.35Wb. Constant $\hat{\varphi_r}$ (left); dynamic $\hat{\varphi_r}$ (right). Dotted red line (reference); solid blue line (measurement)

drive an induction motor. The simulation result proves that the MMC can take place of the traditional VSC. Hence, it is believed that the MMC has a further purpose in the area of the motor drive like wind farms. The issue which $\hat{\varphi_r}$ should be considered as a constant or dynamic in the vector control has been addressed. According to the arithmetic analysis and simulation results, a vector control with considering a constant $\hat{\varphi_r}$ in the inner loop is relatively simple and works well. However, after considering a dynamic $\hat{\varphi_r}$, the vector control loop is decoupled completely, so the vector control with a dynamic $\hat{\varphi_r}$ works more accurately and is better applied for the fast inner loop.

REFERENCES

[1] Y. Ma, Z. Miao, V. R. Disfani, and L. Fan, "A one-step model predictive control for modular multilevel converters," in *PES General Meeting—Conference & Exposition, 2014 IEEE*. IEEE, 2014, pp. 1–5.

[2] Y. Ma, L. Fan, and Z. Miao, "Integrated control and switching strategy for a grid-connected modular multilevel converter."

[3] Y. Han, "Design, modeling, and control of multilevel converter motor drive with modular design and split winding machine," in *Control and Modeling for Power Electronics (COMPEL), 2014 IEEE 15th Workshop on*, June 2014, pp. 1–10.

[4] M. Hagiwara and H. Akagi, "Control and experiment of pulsewidth-modulated modular multilevel converters," *Power Electronics, IEEE Transactions on*, vol. 24, no. 7, pp. 1737–1746, July 2009.

[5] Q. Tu, Z. Xu, and L. Xu, "Reduced switching-frequency modulation and circulating current suppression for modular multilevel converters," *Power Delivery, IEEE Transactions on*, vol. 26, no. 3, pp. 2009–2017, July 2011.

[6] Q. Tu, Z. Xu, H. Huang, and J. Zhang, "Parameter design principle of the arm inductor in modular multilevel converter based hvdc," in *Power System Technology (POWERCON), 2010 International Conference on*, Oct 2010, pp. 1–6.

[7] Y. Zhou, D. Jiang, P. Hu, J. Guo, Y. Liang, and Z. Lin, "A prototype of modular multilevel converters," *Power Electronics, IEEE Transactions on*, vol. 29, no. 7, pp. 3267–3278, July 2014.

[8] X. Lin, K. Ou, Y. Zhang, H. Guo, and Y. Chen, "Simulation and analysis of the operating characteristics of mmc based vsc-mtdc system," in *Innovative Smart Grid Technologies Europe (ISGT EUROPE), 2013 4th IEEE/PES*, Oct 2013, pp. 1–5.

[9] X. Li, W. Liu, Q. Song, H. Rao, and S. Xu, "An enhanced mmc topology with dc fault ride-through capability," in *Industrial Electronics Society, IECON 2013 - 39th Annual Conference of the IEEE*, Nov 2013, pp. 6182–6188.

[10] N. Ahmed, A. Haider, D. Van Hertem, L. Zhang, and H.-P. Nee, "Prospects and challenges of future hvdc supergrids with modular multilevel converters," in *Power Electronics and Applications (EPE 2011), Proceedings of the 2011-14th European Conference on*, Aug 2011, pp. 1–10.

[11] K. Ilves, A. Antonopoulos, S. Norrga, and H.-P. Nee, "Steady-state analysis of interaction between harmonic components of arm and line quantities of modular multilevel converters," *Power Electronics, IEEE Transactions on*, vol. 27, no. 1, pp. 57–68, Jan 2012.

[12] L. Harnefors, A. Antonopoulos, S. Norrga, L. Angquist, and H.-P. Nee, "Dynamic analysis of modular multilevel converters," *Industrial Electronics, IEEE Transactions on*, vol. 60, no. 7, pp. 2526–2537, July 2013.

[13] B. K. Bose, in *Modern Power Electronics and AC Drivers*. PrenticeHall, Englewood Cliffs, New Jersey, 1986.